Journal of Inorganic and General Chemistry
ZAAC
Zeitschrift für anorganische und allgemeine Chemie
www.zaac.wiley-vch.de
RESEARCH ARTICLE

DOI: 10.1002/zaac.202100310

Modelling the coordination environment in α-ketoglutarate dependent oxygenases – a comparative study on the effect of N- vs. O-ligation

Katrin Warm,[a] Dustin Kass,[a] Michael Haumann,[b] Holger Dau,[b] and Kallol Ray*[a]

In various non-heme iron oxygenases the Fe(II) center is coordinated by 2 N and 1 O atoms of the 2-His-2-carboxylate facial triad; however, most artificial model complexes bear only N-based ligands. In an effort to closely mimic the coordination environment in α-ketoglutarate dependent oxygenases, we have now employed the Me_2tacnO ligand (4,7-dimethyl-1-oxa-4,7-diazacyclononane) in the synthesis of the complexes $[(Me_2tacnO)FeCl_2]_2$ (**1-NNO**), $[(Me_2tacnO)FeCl_3]$ (**1 b-NNO**) and $[(Me_2tacnO)Fe(BF)Cl]$ (**2-NNO**; BF = benzoylformate). The weaker donation of the O atom in the ligand was found to result in stronger binding of the ligand in *trans*-position to the O-atom of the ancillary ligand as compared to the corresponding complexes involving the Me_3tacn (1,4,7-trimethyl-1,4,7-triazacyclononane) ligand. Furthermore, by stopped-flow techniques we could detect an intermediate (**3-NNO**) in the reaction of **2-NNO** with O_2. The spectroscopic features of **3-NNO** agree with the involvement of an Fe(IV)-oxo intermediate and hence this study represents the first detection of such an intermediate in the O_2 activation of artificial α-ketoglutarate Fe(II) complexes.

In nature, the activation of the ubiquitous energy source O_2 is performed by various metal-containing enzymes.[1] In many iron-dependent oxidases the active center contains an iron center coordinated by the 2-His-1-carboxylate facial triad. For these enzymes, O_2 activation proceeds, in general, via similar mechanisms, in which O_2 binding is accompanied by the oxidation of cosubstrates resulting in the formation of a potent oxoiron(IV) intermediate species as an active oxidant.[1c] In α-ketoglutarate dependent iron dioxygenases for example, the cosubstrate α-ketoglutarate binds in a bidentate fashion to Fe(II), thereby leaving one vacant binding site available for O_2 binding.[1c,2] The resulting Fe(III) superoxide intermediate formed upon dioxygen activation is believed to undergo an intramolecular oxidative decarboxylation reaction yielding an Fe(IV)-oxo intermediate capable of performing subsequent C–H oxidation reactions (Scheme 1). Even though this intermediate has been thoroughly characterized in the case of enzymes,[2c–h]

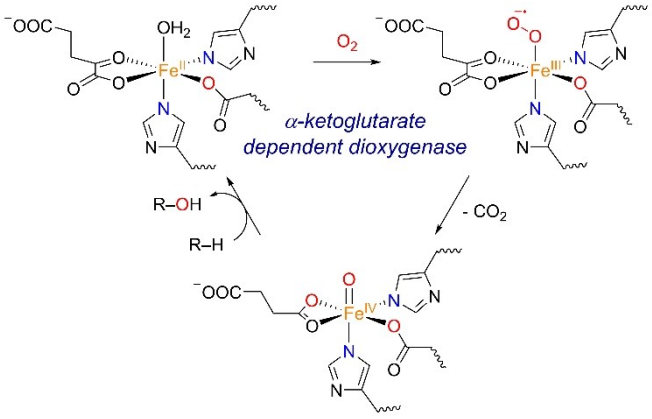

Scheme 1. Top: Simplified catalytic cycle for the O_2 activation and substrate oxidation by α-ketoglutarate dependent oxygenases.

examples of bioinspired Fe(IV)-oxo intermediates obtained by dioxygen activation at biomimetic α-ketocarboxylate Fe(II) centers have stayed elusive to date. Similarly, examples of model complexes capable of catalytic O_2 activation and substrate oxidation reactions using α-ketoacids as cosubstrates are scarce.[3] One recent example is the report of an α-ketocarboxylate Fe(II) complex bearing the facially capping tridentate 1,4,7-triazacyclononane ligand $^{i}Pr_3$tacn (1,4,7-tri-*iso*-propyl-1,4,7-triazacyclononane) that could catalytically oxidize sulfides using dioxygen as an oxidant. Although cycling between Fe^{II} and $Fe^{IV}(O)$ has been proposed as a possible mechanism, spectroscopic trapping of any reactive intermediate was not possible.[3d]

In the present study, we target a directed alteration of a similar triazamacrocyclic framework in Me_3tacn (1,4,7-trimethyl-1,4,7-triazacyclononane) by substitution of one of the nitrogen-

[a] *K. Warm, D. Kass, Prof. Dr. K. Ray*
Institut für Chemie
Humboldt-Universität zu Berlin
Brook-Taylor-Str. 2, 12489 Berlin, Germany
E-mail: kallol.ray@cms.hu-berlin.de
[b] *Dr. M. Haumann, Prof. Dr. H. Dau*
Institut für Physik
Freie Universität Berlin
Arnimallee 14, 14195 Berlin, Germany

Supporting information for this article is available on the WWW under https://doi.org/10.1002/zaac.202100310

donor atoms by oxygen in Me_2tacnO (4,7-dimethyl-1-oxa-4,7-diazacyclononane) and investigate the capability of the corresponding α-ketocarboxylate Fe(II) complexes to perform dioxygen activation. Such oxygen substitution will be not only interesting in the context of understanding nature's preference for using oxygen based donors in dioxygen reduction, it is also expected to affect the stability and reactivity of the oxoiron(IV) intermediate generated upon O_2 activation.[4] In our group we previously reported a dramatic enhancement in the rate of $Fe^{IV}=O$ mediated oxygen atom transfer (OAT) to thioanisole by five orders of magnitude upon switching from a N_4 coordination sphere in TMC (TMC = 1,4,8,11-tetramethyl-1,4,8,11-tetraazacyclotetradecane) to the N_3O coordination sphere in TMCO (TMCO = 4,8,12-trimethyl-1-oxa-4,8,12-triazacyclotetradecane).[4a] Furthermore, incorporation of two sulfur atoms in the cyclam (1,4,8,11-tetraazacyclotetradecane) backbone is shown to result in a change in mechanism to a stepwise proton coupled electron transfer for the $Fe^{IV}=O$ complex supported by the N_2S_2 ligand, in contrast to the tunneling controlled concerted hydrogen atom transfer mechanism for the complex involving the N_4 backbone.[5] Whether a similar replacement of one –NMe group with –O in the ligand backbone can affect the α-ketocarboxylate Fe(II) mediated O_2 activation mechanism is an inherent question, which is investigated in the present study.

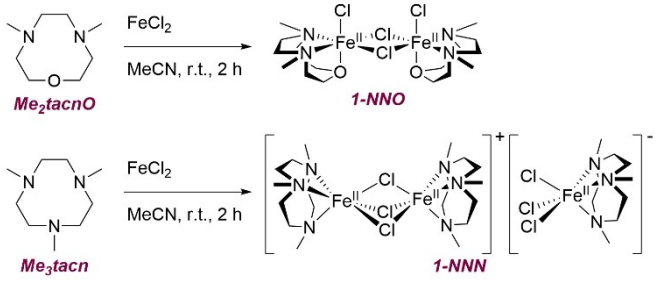

Scheme 2. Synthesis and structures of the **1-NNO** and **1-NNN** complexes from the ligands Me_2tacnO and Me_3tacn, respectively.

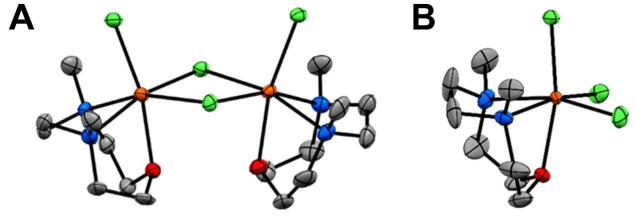

Figure 1. Molecular structures of A) **1-NNO** and B) **1 b-NNO** in ORTEP representation with thermal ellipsoids displayed at 50% probability level; H atoms were omitted for clarity. C: grey, N: blue, O: red, Fe: orange, Cl: green.

The Me_2tacnO (4,7-dimethyl-1-oxa-4,7-diazacyclononane) ligand was synthesized by a modified literature procedure[6] in four steps (Scheme S1) with an overall yield of 62%. Subsequent metalation with iron(II)-chloride yielded a crystalline solid with the composition $[(Me_2tacnO)FeCl_2]$ (**1-NNO**) in analogy to the previously reported $[(Me_3tacn)FeCl_2]$ complex (**1-NNN**).[7] X-ray diffraction (XRD) analysis on single crystals of **1-NNO**, however, revealed some structural differences between the **1-NNN** and **1-NNO** complexes (Scheme 2). While **1-NNN** crystallizes as a $[(Me_3tacn)_2Fe_2Cl_3]^+[(Me_3tacn)FeCl_3]^-$ salt containing a dimeric face-sharing bi-octahedral cation and a monomeric anion,[7] **1-NNO** exists as an electronically neutral $[(Me_2tacnO)_2Fe_2Cl_2(\mu\text{-}Cl)_2]$ dimer (Figure 1, Table 1) in the solid state. The difference between the structures of **1-NNN** and **1-NNO** can be attributed to the presence of terminal Fe–Cl bonds *trans* to the weakly donating O-atom of the Me_2tacnO ligand at distances which are significantly shorter than the Fe–Cl distances in **1-NNN**. The different connectivity between the Fe centers in **1-NNN** and **1-NNO** is reflected in a significantly elongated Fe–Fe distance in **1-NNO** (3.634(2) Å) as compared to that in **1-NNN** (3.006(2) Å).

The dimeric structure of **1-NNO** was found to persist in solution. The ^{1}H NMR spectrum of **1-NNO** in d_3-acetonitrile displays seven paramagnetically broadened signals ranging from 150 to −8 ppm (Figure S1) with integrals consistent with the binding mode of Me_2tacnO found in the XRD structure of **1-NNO**. Electrospray ionization mass spectrometry (ESI-MS) featured signals at *m/z* 290.0 and 533.1 with isotopic distribution patterns matching with $[(Me_2tacnO)(MeCN)FeCl]^+$ (calc. *m/z* 290.1) and $[(Me_2tacnO)_2Fe_2Cl_3]^+$ (calc. *m/z* 533.1), respectively (Figure S2). X-ray absorption spectroscopy (XAS) was also performed on frozen acetonitrile solutions of **1-NNO** to have a closer look into the binding situation in solution. The x-ray absorption near edge structure (XANES) spectrum shows an edge-rise at 7119.9 eV and a pre-edge feature around 7112.6 eV indicative of an Fe(II) center. Extended x-ray absorption fine

Table 1. Average metrical parameters in the solid state structures of **1-NNO**, **1 b-NNO**, **1-NNN**[7] and **1 b-NNN**[8] as obtained from XRD, and the solution state distances of **1-NNO** and **2-NNO** as obtained from EXAFS studies.

Bond	*r* [Å], XRD **1-NNO**	**1-NNN**	**1 b-NNO**	**1 b-NNN**	*r* [Å], EXAFS **1-NNO**	**2-NNO**
Fe–N	2.270	2.202[a] 2.318[b]	2.255	2.247	2.22	2.08
Fe–O	2.217	–	2.220	–		
$Fe–Cl^{terminal}$	2.351	2.451[b]	2.278	2.303	2.32	2.33
$Fe–Cl^{bridging}$	2.493	2.495[a]	–	–		
Fe–Fe	3.634	3.006[a]	–	–	3.46	–

[a] Bond lengths reported for the $[(Me_3tacn)_2Fe_2Cl_3]^+$ cation; [b] bond lengths reported for the $[(Me_3tacn)FeCl_3]^-$ anion.

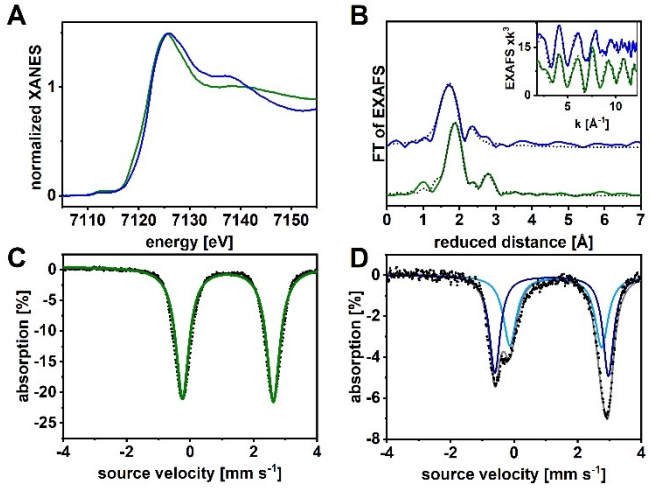

Figure 2. A) XANES spectra of frozen samples of **1-NNO** (green) and **2-NNO** (blue) in acetonitrile; B) Fourier transforms of the EXAFS region of **1-NNO** (green) and **2-NNO** (blue) and simulated data (black dotted lines; for simulation parameters see tables 1, S3); inset shows the k^3-weighted EXAFS signal; C) zero-field Mössbauer spectrum of a frozen sample of **1-NNO** in acetonitrile and simulation for a single species with $\Delta = 1.19\ mm\,s^{-1}$ and $\Delta E_Q = 2.86\ mm\,s^{-1}$; D) zero-field Mössbauer spectrum of a frozen sample of **2-NNO** in acetonitrile and simulation for two major species with $\Delta = 1.285\ mm^{-1}\,s^{-1}$ and $\Delta E_Q = 2.833\ mm^{-1}\,s^{-1}$ (47%) and with $\Delta = 1.143\ mm^{-1}\,s^{-1}$ and $\Delta E_Q = 3.556\ mm^{-1}\,s^{-1}$ (53%).

structure (EXAFS) analysis indicates the presence of 3 N/O scatterers at 2.22 Å, 3 Cl scatterers at 2.32 Å and 1 Fe scatterer at 3.46 Å consistent with the XRD structure. The zero-field Mössbauer spectrum of **1-NNO** in frozen acetonitrile displays a single doublet with an isomer shift (δ) of $1.19\ mm\,s^{-1}$ and a large quadrupole splitting (ΔE_Q) of $2.86\ mm\,s^{-1}$ indicating that both the Fe(II) centers are equivalent and in $S = 2$ spin state (Figure 2A–C).

Next, we targeted the synthesis of an iron(II)-α-ketocarboxylate complex bearing the Me_2tacnO ligand. Reacting **1-NNO** with excess sodium benzoylformate (NaBF) – an α-ketocarboxylate source, which had been successfully employed by Costas *et al.* in the synthesis of the structurally related [(iPr$_3$tacn)Fe(BF)(OTf)] and [(iBu$_3$tacn)$_2$Fe$_2$(μ-BF)$_2$(μ-Cl)](ClO$_4$) complexes[3d] – yielded a dark blue species (**2-NNO**, Scheme 3). An ESI-MS signal at *m/z* 404.2 resulting from [(Me_2tacnO)Fe(BF)(MeCN)]$^+$ (calc. *m/z* 404.1, Figure S3) confirmed the binding of benzoylformate. The absorption spectrum of **2-NNO** shows a broad band centered at 565 nm ($\varepsilon = 60\ M^{-1}\,cm^{-1}$), which is presumably originating from a ligand to metal charge transfer (LMCT) transition associated with the bidentate coordination of α-ketoacids to Fe(II).[9] ^{1}H NMR of the complex displayed several distinguishable signals from −15 to +60 pm (Figure S4), corroborating the paramagnetic nature of the asymmetric complex; however the number of signals indicates that **2-NNO** consists of two isomers in which the α-ketocarboxylate is most likely bound in different orientations (e.g. bidentate ketocarboxylate (**A**) vs terminal carboxylate (**B**) coordinations, see Scheme 3). The zero-field Mössbauer spectrum of **2-NNO** in acetonitrile exhibits two doublets corresponding to the two isomers **A** and **B**. The major species **A** (47%) and **B** (53%) possess isomer shifts of $\Delta(\mathbf{A}) = 1.285\ mm^{-1}\,s^{-1}$ and $\Delta(\mathbf{B}) = 1.143\ mm^{-1}\,s^{-1}$ and quadrupole splittings of $\Delta E_Q(\mathbf{A}) = 2.833\ mm^{-1}\,s^{-1}$ and $\Delta E_Q(\mathbf{B}) = 3.556\ mm^{-1}\,s^{-1}$, respectively, revealing that both species contain high-spin Fe(II) centers (Figure 2 D). The Fe(II) oxidation state in **2-NNO** is, in addition, corroborated by the 7120.6 eV edge-rise and a pre-edge at 7112.1 eV in XANES. EXAFS of **2-NNO** showed 5 N/O ligands at 2.08 Å and 1 Cl ligand at 2.33 Å. In contrast to **1-NNO**, however, no Fe–Fe distance could be detected in EXAFS, hence supporting its formulation as the [(Me_2tacnO)Fe(BF)(Cl)] monomer (Figure 2 A,B).

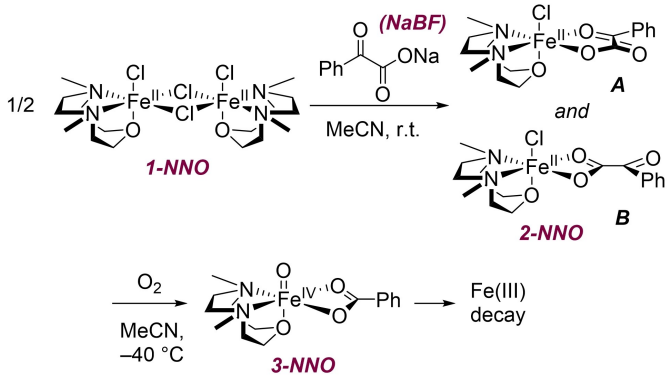

Scheme 3. Synthesis of **2-NNO** and generation of **3-NNO** upon reaction with dioxygen.

In contrast to **1-NNO** which reacts slowly with O_2 over several days to give **1 b-NNO** (Figure 1, Table 1), **2-NNO** reacts with O_2 within seconds in acetonitrile solution even at low temperatures ($t_{1/2} = 20$ s at −40 °C) as evident from the decrease of its characteristic 565 nm band in the absorption spectrum

(Figure S5A). Following the reaction with Mössbauer spectroscopy reveals that while the Fe(II) species **A** is converted to an Fe(III) species with $\Delta = 0.562\ mm\,s^{-1}$ and $\Delta E_Q = 1.011\ mm\,s^{-1}$, the second Fe(II) species **B** did not react with O_2 within the same reaction time (Figure S6). These different reactivities of **A** and **B** plausibly result from the different coordination modes of the ketocarboxylate; the bidentate binding of the ketocarboxylate would place the carbonyl in close proximity to the site of oxygen activation and thus facilitate the oxidation of isomer **A** while a terminal coordination mode of the carboxylate would hinder the oxidation of the more distant α-carbonyl group in **B**. Kinetic studies under stopped-flow conditions at −40 °C showed the formation and the decay of a new species **3-NNO** with an absorption maximum centered around 820 nm (Figure 3). The maximum intensity of this species was obtained after approximately 1.0 s (Figure 3A, inset). The position of the absorption band is consistent with the typical absorption features of oxoiron(IV) centers, indicating that the oxygen activation by **2-NNO** may proceed via a mechanism reminiscent of α-ketoglutarate dependent oxygenases. The infrared spectra of **2-NNO** and its oxidation product (Figure S7) differ mainly in the region between 1750–1500 cm^{-1}, where the characteristic carbonyl stretching vibrations ν(C=O) are expected to appear. These may imply significant structural changes within the benzoylformate ligand upon oxidation of **2-NNO**. ESI-MS spectrum of the reaction mixture of **2-NNO** and O_2 displayed a signal at $m/z = 635.1$ with isotope pattern consistent with $[(Me_2tacnO)_2Fe_2Cl_2(Bz)]^+$ (calc. m/z 635.11, Figure S8) further suggesting the decarboxylation of benzoylformate to benzoate (Bz) during the O_2 reaction.

Unfortunately, the isolation of the corresponding complex **2-NNN** under the same conditions as applied in the synthesis of **2-NNO** was not possible. The UV-Vis spectrum of the green reaction mixture displayed a weak feature at 585 nm ($\varepsilon = 20\ M^{-1}\,cm^{-1}$); the low intensity of this characteristic α-ketocarboxylate Fe(II) LMCT band around 585 nm indicates only partial conversion of **1-NNN** to **2-NNN**. Nevertheless, **2-NNN** was found to react with O_2 as indicated by the immediate decrease of the 585 nm band upon O_2 exposure (Figure S5B). However, the anticipated oxoiron(IV) intermediate could not be detected under stopped-flow conditions (Figure S9), as evident from no changes in the time trace of the absorption @ 820 nm (Figure S9, inset).

In order to diminish the effects of incomplete α-ketocarboxylate binding in **2-NNO** and **2-NNN**, further comparative studies on the reactivities of both systems were performed in presence of excess benzoylformate (20 equiv.). Accordingly, we studied the abilities of **1-NNO** and **1-NNN** to perform catalytic C–H activations on xanthene and O-atom transfer reactions to triphenylphosphine (PPh_3) with O_2 as an oxidant in the presence of excess benzoylformic acid (HBF, 20 equiv.) and excess substrate (20 equiv.). The reaction progress was monitored by ^1H NMR and ^{31}P NMR (Figures S10, S11). While both the complexes were incapable of performing catalytic C–H bond activation reactions, only **2-NNN** could oxidize PPh_3 to $O{=}PPh_3$ catalytically with a turnover number of ≈20 under an O_2 atmosphere within 5 h. Thus, although the iron(II)-α-ketocarboxylate complex **2-NNN** is not formed in high yield, in presence of O_2, it is presumably converted to a transient oxoiron(IV) intermediate, which performs fast OAT to PPh_3. In contrast, **3-NNO** formed in the reaction of **2-NNO** and O_2 is metastable and prefers a one-electron decay to the iron(III) species over a two electron OAT to PPh_3.

To conclude, we evaluated the effect of an N vs O exchange in the N_3 donor ligand tacn in the context of model complexes for α-ketoglutarate dependent oxygenases. The weaker donation by the O atom in Me_2tacnO in contrast to the N_3 donor set in Me_3tacn was found to result in distinct solid state structures for the electronically neutral $[(Me_2tacnO)FeCl_2]_2$ dimer (**1-NNO**) and the $[(Me_3tacn)_2Fe_2Cl_3][(Me_3tacn)FeCl_3]$ salt (**1-NNN**). Furthermore, the N_2O ligation was found to stabilize the bidentate coordination of the α-ketocarboxylate coligand in **2-NNO**, while this coordination mode was only obtained in minor amounts in presence of the N_3 ligand. The better binding of the α-ketocarboxylate to the N_2O complex **1-NNO** hence reveals a possible reason for nature's choice to employ an N_2O donor set in α-ketoglutarate dependent dioxygenases – the weaker donation by the O-atom reduces the electron density on Fe and therefore facilitates the bidentate coordination of the negatively charged α-ketocarboxylate.

While the substitution of N donor atoms by O atoms in the macrocyclic N_4 TMC/cyclam ligands was found to increase the reactivity of the resulting oxoiron(IV) intermediates in previous studies,[4] a different trend is observed upon decreasing the ring size. The oxoiron(IV) species **3-NNO** becomes unstable towards $1e^-$ reduction to Fe(III) species, which prevents catalytic oxygen atom transfer to PPh_3 in presence of oxygen. Nevertheless, the detection of **3-NNO** under stopped-flow conditions represents the first example of an oxoiron(IV) intermediate observed during dioxygen activation by an artificial α-ketocarboxylate Fe(II) complex. Unfortunately, the low thermal stability of the detected intermediate prevented its detailed spectroscopic study and further characterization of its reactivity. Hence, this study represents a relevant step towards the isolation and detailed characterization of intermediates occurring during O_2 activation in α-ketocarboxylate bound Fe(II) complexes by the introduction of weaker donor groups.

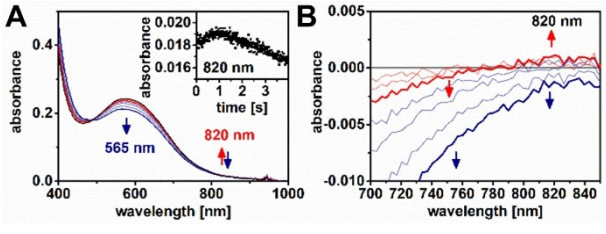

Figure 3. A) Stopped-flow UV-Vis spectra of the reaction of **2-NNO** (black) with O_2 in acetonitrile at −40 °C; inset shows time trace at 820 nm; B) UV-Vis difference spectra after subtraction of the spectrum of **2-NNO** (grey) showing the formation of **3-NNO** (red, after 1.0 s) and its subsequent decay (blue, 4.0 s).

Experimental Section

Chemicals and handling. The chemicals employed were purchased from the companies ABCR, ACROS, SIGMA-ALDRICH and TCI, and used without further purification. Elemental ^{57}Fe with 96.14% isotopic enrichment was purchased from Isoflex (San Francisco, USA) and converted to $^{57}FeCl_2$ according to previously reported procedures.[4,5] Anhydrous solvents (acetonitrile, diethylether, dichloromethane and acetone) were purchased from CARL-ROTH GmbH under the tradename ROTIDRY (>99.5%, <50 ppm H_2O), degassed by freeze-pump-thaw methods prior to use and stored over activated molecular sieves. Deuterated solvents were purchased from EURISO-TOP. Preparation and handling of air or water sensitive compounds were performed under an inert atmosphere using either Schlenk techniques or a glovebox OMNI-LAB 2 from VAC-ATMOSPHERES filled with N_2. Nitrogen and Argon of quality 5.0 were used for this purpose and were purchased from AIR LIQUIDE. Me_2tacnO was synthesized by modified literature procedures.[6d]

***N,N′*-(ethane-1,2-diyl)bis(4-methylbenzenesulfonamide)**. 1,2-ethylenediamine (1.0 equiv., 50 mmol, 3.34 mL) was stirred in 40 mL of H_2O at 20 °C and NaOH (2.4 equiv., 120 mmol, 4.84 g) was added and dissolved while maintaining the reaction temperature at 20 °C using a water bath. *p*-toluenesulfonylchloride (2.0 equiv., 100 mmol, 19.04 g) was dissolved in 110 mL of diethyl ether and the ether solution was added dropwise to the aqueous solution over 2 h under vigorous stirring. The emulsion was left to stir overnight. The white precipitate thus formed was filtered off and washed with diethyl ether. After drying the solid under vacuum, the product was obtained as a white solid (15.14 g, 41.10 mmol, 82%). **^{1}H NMR** (300 MHz, $CDCl_3$): Δ = 7.74–7.68 (m, 4H), 7.31 (d, *J* = 7.9 Hz, 4H), 4.86 (br s, 2H), 3.06 (s, 4H), 2.43 (s, 6H).

4,7-ditosyl-1,4,7-oxadiazonane. *N,N′*-(ethane-1,2-diyl)bis(4-methylbenzenesulfonamide) (1.0 equiv., 5.43 mmol, 2.00 g) and cesium carbonate (2.5 equiv., 13.6 mmol, 4.42 g) were suspended in 80 mL of anhydrous dimethylformamide (DMF) and stirred for 1 h. To the resulting suspension, a solution of diethyleneglycoldi-(*p*-toluenesulfonate) (1.0 equiv., 5.43 mmol, 2.25 g) in 30 mL anhydrous DMF was added slowly over 5 h. The suspension was stirred at room temperature under inert atmosphere for 3 d, then added to an ice-water mixture under vigorous stirring to precipitate the product. Before the ice was completely melted, the product was filtered off and washed carefully with small portions of water. The solid was dried under vacuum overnight. Thus, the product was obtained as white solid (2.33 g, 5.31 mmol, 98%). **^{1}H NMR** (300 MHz, $CDCl_3$) Δ 7.73–7.68 (m, 4H), 7.33 (d, *J* = 8.0 Hz, 4H), 3.94–3.87 (m, 4H), 3.47 (s, 4H), 3.29–3.23 (m, 4H), 2.44 (s, 6H). **ESI-MS** (pos. mode): *m/z* exp. 476.9 ($[M+K]^+$ calc. 477.0915), 502.0 ($[M+Na+MeCN]^+$ calc. 502.1441).

1-oxa-4,7-diazacyclononane (HBr salt). 4,7-ditosyl-1,4,7-oxadiazonane (1.0 equiv., 5.0 mmol, 2.20 g) and phenol (2.0 equiv., 10.0 mmol, 0.94 g) were placed in a 3-necked round-bottom flask equipped with a reflux condenser which was connected to a washing bottle filled with 2 M NaOH solution. The apparatus was flushed with Ar for 3 min, then hydrobromic acid (30% in acetic acid, 120 mL) was added. The mixture was stirred at 80 °C for 16 h, the dark red suspension was cooled to room temperature and the volume of the reaction mixture was reduced to half. The product was precipitated by the addition of acetone to the suspension, the light solid was filtered off, washed several times with cold acetone and dried under vacuum to yield the hydrobromide salt of 1-oxa-4,7-diazacyclononane in ca. 85% purity based on NMR (1.43 g, 4.90 mmol, 82%). **^{1}H NMR** (300 MHz, D_2O) Δ 4.05–3.99 (m, 4H), 3.74 (s, 4H), 3.51–3.46 (m, 4H). **ESI-MS** (pos. mode) *m/z* exp. 131.0 ($[M+H]^+$ calc. 131.1179).

1-oxa-4,7-dimethyl-4,7-diazacyclononane (Me_2tacnO). The hydrobromide salt of 1-oxa-4,7-diazacyclononane (5.51 mmol, 1.61 g), formaldehyde (4.9 mL), formic acid (5.9 mL) and water (0.6 mL) were stirred until the solid was completely dissolved and then refluxed for 1 d. The mixture was cooled to room temperature and neutralized with 2 M NaOH solution until pH > 12. The aqueous solution was extracted 5x with diethyl ether (50 mL each), the organic phases were collected, dried with $MgSO_4$ and the solvent was removed under vacuum. The product Me_2tacnO was obtained as a colourless oil (0.85 g, 5.35 mmol, 97%). **^{1}H NMR** (300 MHz, $CDCl_3$) Δ = 3.75–3.69 (m, 4H, CH_2-O), 2.75–2.68 (m, 8H, CH_2-N), 2.41 (s, 6H, 2 CH_3). **^{13}C NMR** (126 MHz, $CDCl_3$) Δ = 72.95 (CH_2-O), 57.33 (CH_2-N), 57.04 (CH_2-N), 46.56 (CH_3). **ESI-MS** (pos. mode) *m/z* exp. 158.9 ($[M+H]^+$ calc. 159.1492), 339.0 ($[2\,M+Na]^+$ calc. 339.2736), 317.0 ($[2\,M+H]^+$ calc. 317.2917).

$[(Me_2tacnO)FeCl_2]_2$ (1-NNO). Degassed 1-oxa-4,7-dimethyl-4,7-diazacyclononane (1.0 equiv., 3.16 mmol, 0.50 g) was dissolved in 2 mL anhydrous acetonitrile (10 mL) and the solution was added to a suspension of anhydrous iron(II) chloride (1.0 equiv., 0.40 g, 3.16 mmol) in acetonitrile (5 mL). The beige suspension was stirred at 30 °C for 2 h, then filtered to remove excess $FeCl_2$. The solvent was removed under vacuum, the resultant beige solid redissolved in a minimum amount of acetonitrile (ca. 10 mL), the solution was filtered and the complex was precipitated again by the addition of diethylether. The solvent was decanted off and the product was obtained as a light beige solid (0.55 g, 0.96 mmol, 61%) after drying under vacuum. Single crystals suitable for x-ray diffraction analysis could be grown by diffusion of diethylether into a MeCN solution of the complex at −15 °C. The ^{57}Fe-labelled complex for Mössbauer studies was prepared by the same procedure, but using 0.025 g Me_2tacnO, 1 mL MeCN and 20 mg ^{57}Fe-labelled iron(II) chloride. **^{1}H NMR** (300 MHz, CD_3CN): Δ 146.23 (2H, 2*CH*, s, br, $\nu_{1/2} \approx 1200$ Hz), 119.08 (2H, 2*CH*, s, br, $\nu_{1/2} \approx 1150$ Hz), 70.87 (2H, 2*CH*, s, br, $\nu_{1/2} \approx 880$ Hz), 59.38 (2H, 2*CH*, s, br, $\nu_{1/2} \approx 1200$ Hz), 54.59 (2H, 2*CH*, s, br, $\nu_{1/2} \approx 1120$ Hz), 40.12 (6H, 2CH_3, s, br, $\nu_{1/2} \approx 1300$ Hz), −7.50 (2H, 2*CH*, s, br, $\nu_{1/2} \approx 960$ Hz). **CHN analysis**: exp.: C, 33.751/33.757; H, 6.404/6.379; N, 9.784/9.713; calc. [$C_{16}H_{36}Cl_4Fe_2N_4O_2$]: C, 33.72; H, 6.37; Cl, 24.88; Fe, 19.60; N, 9.83; O, 5.61. **ESI-MS** (pos. mode): *m/z* exp 290.0 ($[LFe(MeCN)Cl]^+$ 290.1), 533.1/535.1 ($[L_2Fe_2Cl_3]+$ calc. 533.1/535.1).

$[(Me_2tacnO)FeCl_3]$ (1 b-NNO). Degassed 1-oxa-4,7-dimethyl-4,7-diazacyclononane (1.0 equiv., 0.95 mmol, 0.15 g) and anhydrous iron(III) chloride (1.0 equiv., 0.95 mmol, 0.15 g) were suspended in anhydrous ethanol (5 mL). After 4 h the yellow suspension was filtered and the solvent was removed under vacuum. Recrystallization from an ethanol/diethylether mixture yielded a yellow solid (0.16 g, 0.51 mmol, 53%). Single crystals suitable for x-ray diffraction analysis could be grown by diffusion of diethylether into a EtOH solution of the complex at −15 °C or from the oxidation of the corresponding Fe^{II} complex in air at 20 °C. **CHN analysis**: exp.: C: 29.258, H: 5.662, N: 8.275; calc.: C: 29.99, H: 5.66, N: 8.74.

$[(Me_3tacn)FeCl_2]_2$ ((1-NNN)). 1-NNN was prepared following a literature procedure.[7] Degassed 1,4,7-triazacyclononane (1.0 equiv., 0.88 mmol, 0.15 g) was dissolved in 2 mL anhydrous acetonitrile (2 mL) and the solution was added to a suspension of anhydrous iron(II) chloride (1.0 equiv., 0.11 g, 0.88 mmol) in acetonitrile (1 mL). The beige suspension was stirred at 30 °C for 2 h, then filtered to remove excess $FeCl_2$. The solvent was removed under vacuum, the resultant beige solid redissolved in a minimum amount of acetonitrile (ca. 1 mL), the solution was filtered and the complex was precipitated again by the addition of diethylether. The solvent was decanted off and the product was obtained as a light beige solid (0.23 g, 0.38 mmol, 85%) after drying under vacuum. The identity of the product obtained was confirmed by XRD and comparison of the unit cell to literature and by CHN analysis. Single

crystals suitable for x-ray diffraction analysis could be grown by diffusion of diethylether into a MeCN solution of the complex at room temperature. **CHN analysis**: exp.: C, 35.596; H, 6.848; N, 13.693; calc. $[C_{18}H_{42}Cl_4Fe_2N_6]$: C, 36.27; H, 7.10; N, 14.10.

[(Me_2tacnO)FeCl(BF)] (2-NNO). 1-NNO (0.030 g, 0.05 mmol, 1 equiv.) was dissolved in 2.0 mL anhydrous acetonitrile under N_2 atmosphere. Sodium benzoylformate (NaBF, 0.040 g, 0.2 mmol, 4 equiv.) was added as a solid and the resulting suspension was stirred for 20 h. Excess NaBF was filtered off and the blue solution was added dropwise to diethylether to precipitate the product. After drying of the precipitate under vacuum **2-NNO** was obtained as black solid (0.010 g, 0.033 mmol, 60 %). The ^{57}Fe-labelled complex for Mössbauer studies was prepared by the same procedure, but using 0.010 g labelled **1-NNO**, 1.0 mL MeCN and 20 mg NaBF; after filtering off the excess NaBF the blue solution was directly used for the preparation of Mössbauer samples. **^{1}H NMR** (300 MHz, Acetonitrile-d_3) Δ 58.38 (s, 1H, Ar–H), 53.66 (s, 1H, Ar–H), 48.02 (s, 1H, Ar–H), 46.05 (s, 2H, Ar–H), 43.75 (s, 1H, Ar–H), 42.11 (s, 1H, Ar–H), 38.10 (d, 2H, Ar–H), 29.60 (s, 1H, Ar–H), 10.08 (br m, J = 1046.9 Hz, 36H, 2xMe_2tacnO), −1.84 (s, 1H,, Ar–H), −4.14 (s, 1H, Ar–H). **CHN analysis**: exp.: C, 52.486/52.599; H, 4.733/4.688; N, 5.213/5.159; calc. $[C_{16}H_{23}ClFeN_2O_4 \cdot NaBF]$: C, 50.50; H, 4.94; N, 4.91. **UV-Vis**: ε_{max} (565 nm) = 60 M^{-1} cm^{-1}.

[(Me_3tacn)FeCl(BF)] (2-NNN). 1-NNN (0.030 g, 0.05 mmol, 1.0 equiv.) was dissolved in 2.0 mL anhydrous acetonitrile under N_2 atmosphere. Sodium benzoylformate (NaBF, 0.090 g, 0.50 mmol, 10 equiv.) was added as a solid and the resulting suspension was stirred for 20 h. Excess NaBF was filtered off and the green solution was added dropwise to diethylether to precipitate the product. After drying of the precipitate under vacuum, a dark green solid was obtained (0.01 g). **UV-Vis**: ε_{max} (585 nm) = 20 M^{-1} cm^{-1}.

O_2 reactivity studies. For UV-Vis studies, 10 mM stock solutions of the complexes **1-NNN** or **1-NNO** respectively were prepared in acetonitrile by dissolving 0.040 g of **1-NNN** or 0.041 g of **1-NNO** in 0.40 mL of anhydrous acetonitrile. 0.10 mL of the respective stock solution was added via syringe to a O_2-saturated solution of acetonitrile (1.00 mL) in a cuvette which was precooled to −40 °C. The decay of the 565 nm or 585 nm UV-Vis feature was followed by UV-Vis spectroscopy. For stopped-flow studies, the sample cell was precooled to −40 °C. Inside of the cooled cell, an O_2-saturated solution and a solution of the complex (0.040–0.050 g in 3.0 mL) in anhydrous, degassed acetonitrile were mixed.

Catalysis studies. Stock solutions of the complexes were prepared by dissolving 0.041 mg of **1-NNN** or 0.040 mg of **1-NNO** in 1.00 mL anhydrous d_3-acetonitrile under N_2 atmosphere. The complex (5.0 mol %, 0.10 mL stock solution, 1.0 μmol Fe^{II}) and HBF (40 μmol, 6.0 mg) were dissolved in 1.0 mL d_3-acetonitrile under N_2 atmosphere. To this solution, the substrate (20 μmol, 0.010 g PPh_3 or 0.072 g xanthene) and 1,3,5-trimethoxybenzene (1.0 μmol, 0.33 mg) as standard were added. The mixture was opened to air and stirred for 15 min, then transferred to an NMR tube. After 20–30 min, NMR spectra of the reaction mixtures were measured. The NMR measurement was repeated after 2 h and 5 h for PPh_3 oxidation. Control experiments in the absence of **1-NNN** (or with $FeCl_2$ or $FeCl_3$ salts instead of **1-NNN**) did not show any oxidation of the substrates.

Elemental analysis. All elemental analyses were performed by the analytical service of the Institut für Chemie of the Humboldt-Universität zu Berlin. The percentages of Carbon, Hydrogen and Nitrogen were determined using an HEKAtech EURO EA 3000 analyzer.

Nuclear magnetic resonance spectroscopy. All NMR spectra were recorded using a BRUKER 300 DPX spectrometer equipped with a cryostat. Those of ^{1}H and ^{31}P nuclei were recorded in deuterated solvents, and chemical shifts (ppm) referenced against residual protic solvent peaks.

Electrospray ionization mass spectrometry. ESI-MS spectra of organic molecules and inorganic complexes in solution were recorded by using an ADVION EXPRESSION CMS spectrometer (using the default ionization conditions of the instrument) and spectra in positive and negative mode were collected in parallel; acetonitrile was used as an eluent. For thermally unstable complexes, the freshly thawed solutions were directly injected into the instrument while the ionization source temperature was decreased to 50 °C. The analysis of the data was carried out with the ADVION DATA EXPRESS Version 6.0.11.3.

Infrared spectroscopy. Infrared spectra of **2-NNO** and its reaction product with oxygen were collected with an Agilent Cary 630 FT-IR spectrometer by the use of the Attenuated Total Reflection (ATR) setup.

Stopped-flow UV/Vis spectroscopy. Stopped-flow UV/vis measurements were performed with an SFM4000 from BioLogic SAS using a cryo-stopped-flow set-up which is equipped with a Hamatsu L10290 high power UV/vis fiber light source and a TIDAS S 300 K VIS/NIR 3011 spectrometer. Instrument tuning and data handling were performed with BioKine Version 4.73 supplied by BioLogic. The pathlength of the installed cuvette is 1 mm. The dead time lies in between 1 to 3 ms depending on flow rate (8–12 ml/s) and integration time.

Single crystal x-ray structure determinations. For the determination of the x-ray crystal structure of the complex data collection was performed at 100 K on a BRUKER D8 VENTURE diffractometer by using Mo Kα radiation (λ = 0.71073 Å). Multi-scan absorption corrections implemented in SADABS[10] were applied to the data. The structure was solved by intrinsic phasing method (SHELXT 2014/5)[11] and refined by full matrix least square procedures based on F_2 with all measured reflections (SHELXL-2018/3)[12] in the graphical user interface SHELXle[13]) with anisotropic temperature factors for all non-hydrogen atoms. All hydrogen atoms were added geometrically and refined by using a riding model. The XRD structures of **1-NNO** and **1 b-NNO** were refined as inversion twins. **CCDC** 2110036 (**1-NNO**) and 2109743 (**1 b-NNO**) contain the supplementary crystallographic data for this paper. These data can be obtained free of charge from the Cambridge Crystallographic Data Center via www.ccdc.cam.ac.uk/data_request/cif.

Mössbauer spectroscopy. Mössbauer spectra in the absence of magnetic field were recorded on a SEECO MS6 spectrometer that comprises the following instruments: a JANIS CCS-850 cryostat, including a CTI-CRYOGENICS closed cycle 10 K refrigerator, and a CTI-CRYOGENICS 8200 helium compressor. The cold head and sample mount are equipped with calibrated DT-670-Cu-1.4 L silicon diode temperature probes and heaters. Temperature is controlled by a LAKESHORE 335 temperature controller. Spectra are recorded using a LND-45431 Kr gas proportional counter with beryllium window connected to the SEECO W204 γ-ray spectrometer that includes a high voltage supply, a 10 bit and 5 μs ADC and two single channel analyzers. Motor control and recording of spectra is taken care of by the W304 resonant γ-ray spectrometer. For the reported spectra a RIVERTEC MCO7.114 source (^{57}Co in Rh matrix) with an activity of about 1 GBq was used. All spectra were recorded in a plastic sample holder with a frozen solution sample at 35 K and data were accumulated for about 24 hours.

X-ray absorption spectroscopy. XAS at the Fe K-edge was performed at beamline KMC-3 at the BESSY-II synchrotron (Helmholtz Center Berlin, Germany) as described earlier[5b] using a set-up including a Si[111] double-crystal monochromator, a 13-element energy-resolving Si-drift detector (RaySpec) for x-ray fluorescence

monitoring, and DXP-XMAP pulse-processing electronics (XIA). Samples were held at 20 K in a liquid-helium cryostat (Oxford). The energy axis of the monochromator was calibrated (accuracy ±0.1 eV) using the K-edge spectrum of an iron metal foil (fitted reference energy of 7112 eV in the first derivative spectrum). The spot size on the samples was ca. 1.5×3.0 mm (vertical×horizontal) as set by a focusing mirror and slits. x-ray fluorescence spectra were collected using a continuous scan mode of the monochromator (scan duration ~10 min). Up to 6 scans were averaged (1–2 scans per sample spot) for signal-to-noise ratio improvement. XAS data were processed (dead-time correction, background subtraction, normalization) to yield XANES and EXAFS spectra using our earlier described procedures and in-house software.[14] k^3-weighted EXAFS spectra were simulated with in-house software and phase functions from FEFF9 ($S_0^2 = 0.8$).[15] EXAFS simulation results are tabulated in Table S3.

Acknowledgements

This work was funded by the Deutsche Forschungsgemeinschaft (DFG, German Research Foundation) under Germany's Excellence Strategy - EXC 2008-390540038 – UniSysCat to K.R., and H.D. and the Heisenberg-Professorship to K.R.. K.W. also thanks Einstein Foundation Berlin (ESB) – Einstein Center of Catalysis (EC^2) for its support. We acknowledge the Helmholtz Zentrum Berlin (HZB) for providing experimental infrastructure and allocating beamtime at beamline KMC-3 of the BESSY synchrotron; we thank Ivo Zizak and further BESSY staff for their support. Open Access funding enabled and organized by Projekt DEAL.

Conflict of Interest

The authors declare no conflict of interest.

Keywords: Non-heme ligand · iron oxygenases · model complexes · oxoiron(IV) intermediate · O_2-activation

[1] a) E. I. Solomon, D. E. Heppner, E. M. Johnston, J. W. Ginsbach, J. Cirera, M. Qayyum, M. T. Kieber-Emmons, C. H. Kjaergaard, R. G. Hadt, L. Tian, *Chem. Rev.* **2014**, *114*, 3659–3853; b) A. J. Jasniewski, L. Que, *Chem. Rev.* **2018**, *118*, 2554–2592; c) S. Kal, L. Que, *J. Biol. Inorg. Chem.* **2017**, *22*, 339–365; d) S. C. Peck, W. A. van der Donk, *J. Biol. Inorg. Chem.* **2017**, *22*, 381–394.

[2] a) S. Sinnecker, N. Svensen, E. W. Barr, S. Ye, J. M. Bollinger, F. Neese, C. Krebs, *J. Am. Chem. Soc.* **2007**, *129*, 6168–6179; b) C. Krebs, D. Galonić Fujimori, C. T. Walsh, J. M. Bollinger, *Acc. Chem. Res.* **2007**, *40*, 484–492; c) J. M. Bollinger Jr., J. C. Price, L. M. Hoffart, E. W. Barr, C. Krebs, *Eur. J. Inorg. Chem.* **2005**, *2005*, 4245–4254; d) J. C. Price, E. W. Barr, B. Tirupati, J. M. Bollinger, C. Krebs, *Biochemistry* **2003**, *42*, 7497–7508; e) P. J. Riggs-Gelasco, J. C. Price, R. B. Guyer, J. H. Brehm, E. W. Barr, J. M. Bollinger, C. Krebs, *J. Am. Chem. Soc.* **2004**, *126*, 8108–8109; f) L. M. Hoffart, E. W. Barr, R. B. Guyer, J. M. Bollinger, C. Krebs, *Proc. Natl. Acad. Sci. USA* **2006**, *103*, 14738–14743; g) B. E. Eser, E. W. Barr, P. A. Frantom, L. Saleh, J. M. Bollinger, C. Krebs, P. F. Fitzpatrick, *J. Am. Chem. Soc.* **2007**, *129*, 11334–11335; h) D. P. Galonić, E. W. Barr, C. T. Walsh, J. M. Bollinger, C. Krebs, *Nat. Chem. Biol.* **2007**, *3*, 113–116.

[3] a) D. Sheet, P. Halder, T. K. Paine, *Angew. Chem. Int. Ed.* **2013**, *52*, 13314–13318; *Angew. Chem.* **2013**, *125*, 13556–13560; b) O. Das, S. Chatterjee, T. K. Paine, *J. Biol. Inorg. Chem.* **2013**, *18*, 401–410; c) D. Sheet, T. K. Paine, *Chem. Sci.* **2016**, *7*, 5322–5331; d) B. N. Sánchez-Eguía, J. Serrano-Plana, A. Company, M. Costas, *Chem. Commun.* **2020**, *56*, 14369–14372.

[4] a) I. Monte Pérez, X. Engelmann, Y.-M. Lee, M. Yoo, E. Kumaran, E. R. Farquhar, E. Bill, J. England, W. Nam, M. Swart, K. Ray, *Angew. Chem. Int. Ed.* **2017**, *56*, 14384–14388; *Angew. Chem.* **2017**, *129*, 14576–14580; b) C. Wegeberg, M. L. Skavenborg, A. Liberato, J. N. McPherson, W. R. Browne, E. D. Hedegaard, C. J. McKenzie, *Inorg. Chem.* **2021**, *60*, 1975–1984.

[5] a) J. Deutscher, P. Gerschel, K. Warm, U. Kuhlmann, S. Mebs, M. Haumann, H. Dau, P. Hildebrandt, U.-P. Apfel, K. Ray, *Chem. Commun.* **2021**, *57*, 2947–2950; b) D. Kass, T. Corona, K. Warm, B. Braun-Cula, U. Kuhlmann, E. Bill, S. Mebs, M. Swart, H. Dau, M. Haumann, P. Hildebrandt, K. Ray, *J. Am. Chem. Soc.* **2020**, *142*, 5924–5928.

[6] a) R. Delgado, J. J. R. F. Da Silva, M. T. S. Amorim, M. F. Cabral, S. Chaves, J. Costa, *Anal. Chim. Acta* **1991**, *245*, 271–282; b) M. F. Cabral, J. Costa, R. Delgado, J. J. R. F. Da Silva, M. F. Vilhena, *Polyhedron* **1990**, *9*, 2847–2857; c) P. J. Wilson, A. J. Blake, P. Mountford, M. Schröder, *Inorg. Chim. Acta* **2003**, *345*, 44–52; d) A. P. Cole, V. Mahadevan, L. M. Mirica, X. Ottenwaelder, T. D. P. Stack, *Inorg. Chem.* **2005**, *44*, 7345–7364.

[7] A. C. Moreland, T. B. Rauchfuss, *Inorg. Chem.* **2000**, *39*, 3029–3036.

[8] G. C. Silver, W. C. Trogler, *J. Am. Chem. Soc.* **1995**, *117*, 3983–3993.

[9] a) R. Y. N. Ho, M. P. Mehn, E. L. Hegg, A. Liu, M. J. Ryle, R. P. Hausinger, L. Que, *J. Am. Chem. Soc.* **2001**, *123*, 5022–5029; b) M. P. Mehn, K. Fujisawa, E. L. Hegg, L. Que, *J. Am. Chem. Soc.* **2003**, *125*, 7828–7842.

[10] G. M. Sheldrick, SADABS, Version 2.05. A Software for Empirical Absorption Correction, University of Göttingen, Germany, **2002**.

[11] G. Sheldrick, *Acta Cryst. Sect. A* **2015**, *71*, 3–8.

[12] G. Sheldrick, *Acta Cryst. Sect. C* **2015**, *71*, 3–8.

[13] C. B. Hubschle, G. M. Sheldrick, B. Dittrich, *J. Appl. Crystallogr.* **2011**, *44*, 1281–1284.

[14] H. Dau, P. Liebisch, M. Haumann, *Anal. Bioanal. Chem.* **2003**, *376*, 562–583.

[15] J. J. Rehr, J. J. Kas, F. D. Vila, M. P. Prange, K. Jorissen, *Phys. Chem. Chem. Phys.* **2010**, *12*, 5503–5513.

Manuscript received: October 16, 2021
Revised manuscript received: December 30, 2021

